

Optimization of a spectrum splitter using differential evolution algorithm for solar cell applications

Li Fan,¹ Muhammad Faryad,² Greg D. Barber,³ Thomas E. Mallouk,³
Peter B. Monk,¹ and Akhlesh Lakhtakia²

¹Department of Mathematical Sciences, University of Delaware, Newark, DE 19716

²Nanoengineered Metamaterials Group, Department of Engineering Science and Mechanics,
Pennsylvania State University, University Park, PA 16802

³Department of Chemistry, Pennsylvania State University, University Park, PA 16802

ABSTRACT

A spectrum splitter can be used to spatially multiplex different solar cells that have high efficiency in mutually exclusive parts of the solar spectrum. We investigated the use of a surface-relief grating made of dielectric materials for specularly transmitting one part of the solar spectrum while the other part is transmitted non-specularly and the total reflectance is very low. A combination of (i) the rigorous coupled-wave approach for computing the reflection and transmission coefficients of the grating and (ii) the differential evolution algorithm for optimizing the grating shape was devised as a design tool. We used this tool to optimize two candidate gratings and obtained definite improvements to the initial guesses for the structural and constitutive parameters. Significant spectrum splitting can be achieved if the angle of incidence does not exceed 15° .

1. INTRODUCTION

The efficiency of a solar cell varies with the (free-space) wavelength. Some semiconductors are more efficient harvesters of solar energy at longer wavelengths, other at shorter wavelengths.¹ If the incident solar light could be split such that light below a cutoff wavelength is directed to a solar cell that is efficient in that wavelength range, while light at wavelengths above the cutoff wavelength is directed to another solar cell that is efficient in that spectral regime, then maximal harvesting of solar energy could become possible. So a spectrum splitter could be used to spatially multiplex different solar cells that have high efficiency in mutually exclusive parts of the solar spectrum. This fundamental concept proposed in 1955¹ is still a hot topic for research.²⁻⁶

Recent experimental work has focused on the spectrum-splitting concept using a hybrid arrangement of silicon and dye-sensitized solar cells.⁵ In these experiments, a bandstop filter on the entry pupil of a dye-sensitized solar cell was used to reflect and concentrate near-infrared light onto a silicon p-n junction cell. As an alternative to that approach, we theoretically examined the use of a surface-relief grating made of dielectric materials for specularly transmitting light of longer wavelengths while light of shorter wavelengths predominately transmitted non-specularly. Such a grating could be placed on top of a lens to selectively focus and concentrate long-wavelength light onto a silicon absorber, while deflecting short-wavelength visible light to a back plane of a large-area absorber such as a dye-sensitized solar cell. An obvious question arises: how to optimize the geometry and material constituents of a spectrum splitter in order to obtain the best performance. In this paper, we show that a combination of the rigorous coupled-wave approach (RCWA) to determine the reflection and transmission characteristics of the grating^{7,8} with the differential evolution algorithm (DEA) for optimizing the geometry and the refractive indexes of the material constituents,⁹⁻¹¹ gives a useful design tool.

Further author information: Corresponding author (LF). E-mail: fanli@udel.edu, Telephone: +1 302 831 0518. MF is presently with the Department of Physics, Lahore University of Management Sciences, Lahore 54792, Pakistan.

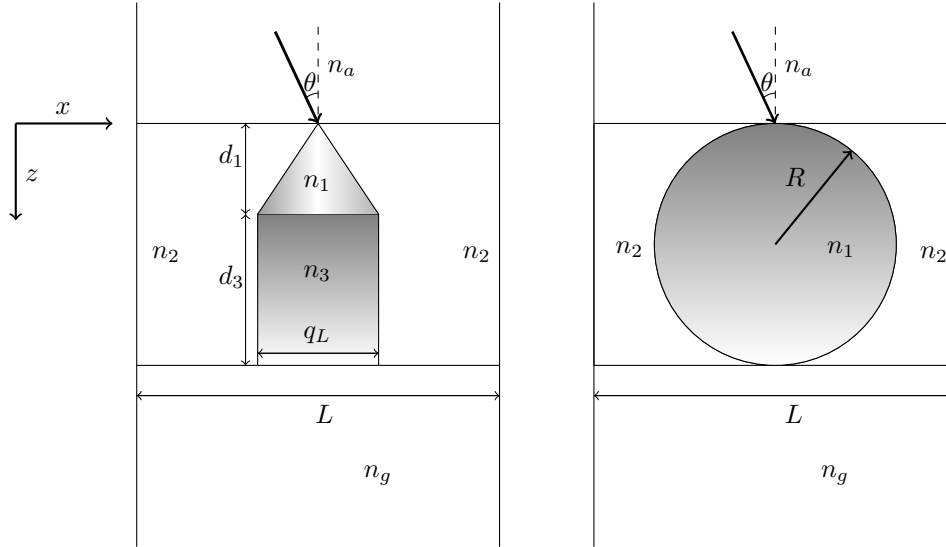


Figure 1. Two candidates for splitting the solar spectrum. The splitter on the left side is predicted to work well, but will pose some manufacturing challenges. The splitter on the right side is predicted to be sensitive to the angle of incidence of light with respect to the z axis, but will be easier to manufacture than the one of the left.

Our approach to splitter design is to apply optimization to improve a basic design that already shows promise of spectrum splitting. We examined the two candidate splitters shown in Fig. 1. For both candidates, the grating lines were taken to be infinitely long and parallel to the y axis in a Cartesian coordinate system, the grating was assumed to be of infinite extent along the x axis with period L , the height of the grating along the z axis was set equal to d , the half space $z < 0$ was taken to be occupied by air with refractive index $n_a = 1$, and the half space $z > d$ was taken to be occupied by glass with refractive index n_g . Light was taken to be incident on either splitter from the half space $z < 0$, the wave vector of the incident light lying wholly in the xz plane and oriented at an angle θ with respect to the z axis, where θ is taken to be positive when measured counter-clockwise and negative when measured clockwise.

The free parameters for the triangle-topped rectangular grating were taken as: L , q_L , d_1 , $d_3 = d - d_1$, n_1 , and n_2 (n_3 is assumed to be fixed). The free parameters for the grating with lines of circular cross section were taken as: L , $R = d/2$, n_1 , and n_2 . Useful improvements to the basic design were obtained. Application of the DEA indicated that significant spectrum splitting can be achieved if the angle of incidence $\theta \in [-15^\circ, 15^\circ]$.

The paper proceeds as follows. In Section 2, we briefly outline the RCWA used to predict the transmission and reflection coefficients of a grating. The DEA for optimization is described in Sec. 3. For both candidate splitters, numerical results are provided in Sec. 4, allowing us to predict the degree of spectrum splitting. Concluding remarks are presented in Sec. 5.

Vectors are denoted in boldface. The Cartesian unit vectors are denoted as $\hat{\mathbf{u}}_x$, $\hat{\mathbf{u}}_y$, and $\hat{\mathbf{u}}_z$. During the application of the RCWA, an $\exp(-i\omega t)$ dependence on time t was assumed for all electric and magnetic field phasors, with $i = \sqrt{-1}$ and ω as the angular frequency. Furthermore, the free-space wavenumber is denoted by $k_0 = \omega\sqrt{\varepsilon_0\mu_0}$ and the free-space wavelength by $\lambda_0 = 2\pi/k_0$, with ε_0 as the permittivity and μ_0 as the permeability of free space.

2. RIGOROUS COUPLED-WAVE APPROACH

In the half-space $z \leq 0$, incident sunlight is modeled as a spectrum of plane waves propagating in the xz plane at an angle θ with respect to the z axis. Then, the electric field phasor of the incident plane wave of wavelength λ_0 may be written in terms of Floquet harmonics as⁸

$$\mathbf{E}_{inc}(x, z, \lambda_0) = \sum_{n \in \mathbb{Z}} \left[\hat{\mathbf{u}}_y a_s^{(n)}(\lambda_0) + \mathbf{p}_n^{a+}(\lambda_0) a_p^{(n)}(\lambda_0) \right] \exp \left\{ i \left[k_x^{(n)}(\lambda_0)x + k_{za}^{(n)}(\lambda_0)z \right] \right\}, \quad z \leq 0, \quad (1)$$

where $\mathbb{Z} = \{0, \pm 1, \pm 2, \dots\}$; the subscripts p and s represent the p - and s -polarization states, respectively; and

$$\mathbf{p}_n^{a\pm}(\lambda_0) = \frac{\mp k_{za}^{(n)} \hat{\mathbf{u}}_x + k_x^{(n)} \hat{\mathbf{u}}_z}{k_0 n_a}, \quad (2)$$

$$k_x^{(n)}(\lambda_0) = k_0 n_a \sin \theta + 2\pi n/L, \quad (3)$$

$$k_{za}^{(n)}(\lambda_0) = \begin{cases} +\sqrt{k_0^2 n_a^2 - (k_x^{(n)})^2}, & k_0^2 n_a^2 > (k_x^{(n)})^2, \\ +i\sqrt{(k_x^{(n)})^2 - k_0^2 n_a^2}, & k_0^2 n_a^2 < (k_x^{(n)})^2. \end{cases} \quad (4)$$

The corresponding electric field phasors of the reflected and transmitted plane waves may be stated as⁸

$$\mathbf{E}_{refl}(x, z, \lambda_0) = \sum_{n \in \mathbb{Z}} \left[\hat{\mathbf{u}}_y r_s^{(n)}(\lambda_0) + \mathbf{p}_n^{a-}(\lambda_0) r_p^{(n)}(\lambda_0) \right] \exp \left\{ i \left[k_x^{(n)}(\lambda_0) x - k_{za}^{(n)}(\lambda_0) z \right] \right\}, \quad z < 0, \quad (5)$$

$$\mathbf{E}_{tr}(x, z, \lambda_0) = \sum_{n \in \mathbb{Z}} \left[\hat{\mathbf{u}}_y t_s^{(n)}(\lambda_0) + \mathbf{p}_n^{g+}(\lambda_0) t_p^{(n)}(\lambda_0) \right] \exp \left\{ i \left[k_x^{(n)}(\lambda_0) x + k_{zg}^{(n)}(\lambda_0) (z - d) \right] \right\}, \quad z > d, \quad (6)$$

where

$$\mathbf{p}_n^{g\pm}(\lambda_0) = \frac{\mp k_{zg}^{(n)} \hat{\mathbf{u}}_x + k_x^{(n)} \hat{\mathbf{u}}_z}{k_0 n_g}, \quad (7)$$

$$k_{zg}^{(n)}(\lambda_0) = \begin{cases} +\sqrt{k_0^2 n_g^2 - (k_x^{(n)})^2}, & k_0^2 n_g^2 > (k_x^{(n)})^2 \\ +i\sqrt{(k_x^{(n)})^2 - k_0^2 n_g^2}, & k_0^2 n_g^2 < (k_x^{(n)})^2. \end{cases} \quad (8)$$

Components of the reflected and transmitted light in Eqs. (1), (5), and (6) corresponding to $n = 0$ are termed specular, all the remaining components (when $n \neq 0$) being called non-specular. An optimal splitter would transmit 100% of the energy to specular modes above a specified cutoff wavelength λ_c , and 100% of the energy to non-specular modes for wavelengths below λ_c . Obviously, an ideal splitter cannot be obtained in practice.

The incidence amplitudes $\{a_p^{(n)}(\lambda_0), a_s^{(n)}(\lambda_0)\}_{n \in \mathbb{Z}}$ are presumed known, with the proviso that $a_p^{(n)}(\lambda_0) = a_s^{(n)}(\lambda_0) = 0 \forall n \neq 0$. However, $a_p^{(0)}(\lambda_0) \neq 0$ and $a_s^{(0)}(\lambda_0) = 0$ for a p -polarized incident plane wave, and $a_p^{(0)}(\lambda_0) = 0$ and $a_s^{(0)}(\lambda_0) \neq 0$ for an s -polarized incident plane wave. The corresponding reflection amplitudes $\{r_p^{(n)}(\lambda_0), r_s^{(n)}(\lambda_0)\}_{n \in \mathbb{Z}}$ and transmission amplitudes $\{t_p^{(n)}(\lambda_0), t_s^{(n)}(\lambda_0)\}_{n \in \mathbb{Z}}$ have to be determined by solving a boundary-value problem.

That task is best accomplished by implementing the RCWA algorithm described in detail elsewhere.^{7,12} Briefly, the relative permittivity $\varepsilon(x, z, \lambda_0)$ in the region $0 \leq z \leq d$ is expanded as a Fourier series with respect to x , viz.,

$$\varepsilon(x, z, \lambda_0) = \sum_{n \in \mathbb{Z}} \epsilon^{(n)}(z, \lambda_0) \exp(i2\pi n x/L), \quad z \in (0, d),$$

where the coefficients $\epsilon^{(n)}(z, \lambda_0)$ have to be determined for each candidate splitter separately. The electric and magnetic field phasors in the grating region $0 < z < d$ may then be written in terms of Floquet harmonics as

$$\begin{aligned} \mathbf{E}(x, z, \lambda_0) &= \sum_{n \in \mathbb{Z}} \mathbf{e}^{(n)}(z, \lambda_0) \exp \left[i k_x^{(n)}(\lambda_0) x \right], \quad z \in (0, d), \\ \mathbf{H}(x, z, \lambda_0) &= \sum_{n \in \mathbb{Z}} \mathbf{h}^{(n)}(z, \lambda_0) \exp \left[i k_x^{(n)}(\lambda_0) x \right], \quad z \in (0, d). \end{aligned}$$

Substitution of these expressions into the frequency-domain Maxwell equations gives a coupled system of ordinary differential equations in z for the amplitudes $\mathbf{e}^{(n)}(z, \lambda_0)$ and $\mathbf{h}^{(n)}(z, \lambda_0)$, $n \in (-\infty, \infty)$.

In order to obtain a numerically tractable system, the infinite series appearing in these expressions are truncated so that $n \in [-N_t, N_t]$, thereby obtaining $2N_t + 1$ coupled linear ordinary differential equations. To solve this system, the coefficients $\varepsilon^{(n)}(z, \lambda_0)$ are further approximated by piecewise constant functions in z using a uniform partition of the grating into horizontal layers. The resulting boundary-value problem is solved by a stabilized marching scheme.^{7,8,12}

No depolarization can occur for the chosen boundary-value problem. For an r -polarized incident plane wave, $r \in \{s, p\}$, the modal reflectances are given by

$$R_{rr}^{(n)}(\lambda_0) = \left| \frac{r_r^{(n)}(\lambda_0)}{a_r^{(0)}(\lambda_0)} \right|^2 \frac{\text{Re} \left[k_{za}^{(n)}(\lambda_0) \right]}{k_{za}^{(0)}(\lambda_0)} \quad (9)$$

and the modal transmittances by

$$T_{rr}^{(n)}(\lambda_0) = \left| \frac{t_r^{(n)}(\lambda_0)}{a_r^{(0)}(\lambda_0)} \right|^2 \frac{\text{Re} \left[k_{zg}^{(n)}(\lambda_0) \right]}{k_{za}^{(0)}(\lambda_0)}. \quad (10)$$

We also defined the following quantities for convenience of later discussion:

$$R_{rr}^{n \neq 0}(\lambda_0) = \sum_{n=-N_t}^{N_t} \left[R_{rr}^{(n)}(\lambda_0) \right] - R_{rr}^{(0)}(\lambda_0), \quad r \in \{s, p\}, \quad (11)$$

$$T_{rr}^{n \neq 0}(\lambda_0) = \sum_{n=-N_t}^{N_t} \left[T_{rr}^{(n)}(\lambda_0) \right] - T_{rr}^{(0)}(\lambda_0), \quad r \in \{s, p\}, \quad (12)$$

$$R^{n \neq 0}(\lambda_0) = \frac{1}{2} \left[R_{ss}^{n \neq 0}(\lambda_0) + R_{pp}^{n \neq 0}(\lambda_0) \right], \quad (13)$$

$$T^{n \neq 0}(\lambda_0) = \frac{1}{2} \left[T_{ss}^{n \neq 0}(\lambda_0) + T_{pp}^{n \neq 0}(\lambda_0) \right], \quad (14)$$

$$R^{(0)}(\lambda_0) = \frac{1}{2} \left[R_{ss}^{(0)}(\lambda_0) + R_{pp}^{(0)}(\lambda_0) \right], \quad (15)$$

$$T^{(0)}(\lambda_0) = \frac{1}{2} \left[T_{ss}^{(0)}(\lambda_0) + T_{pp}^{(0)}(\lambda_0) \right]. \quad (16)$$

We used layers of thickness 5 nm for the piecewise-uniform approximation of the coefficients $\varepsilon^{(n)}(z, \lambda_0)$ for $z \in (0, d)$, and we selected $N_t = 14$, after ensuring that principle of conservation of energy¹² was satisfied with an error less than 0.01%.

3. DIFFERENTIAL EVOLUTION ALGORITHM

We implemented the DEA^{9,10} to seek an optimal design for each of the two candidate splitters shown in Fig. 1. The DEA is a genetic algorithm that iteratively improves a candidate solution with regard to a given measure of quality, given an initial guess in the search space together with several other candidate solutions. The algorithm attempts to avoid local minimums by stochastic choices of the updates at each step. A large space of candidate solutions can be searched, but a global minimum is not guaranteed. It is helpful to limit the search space and have a good initial choice of the free parameters. Therefore, we used this algorithm in conjunction with the conclusions gleaned from inspection of RCWA results for both candidate splitters.¹¹

In brief, let $\mathbf{v} = (v_1, v_2, v_3, \dots, v_{\tilde{n}})$ denote a point in the search space $\mathcal{S} \subset \mathbb{R}^{\tilde{n}}$ for the free parameters that can be varied to obtain an optimal design, \tilde{n} being the number of components of \mathbf{v} . The objective is to find \mathbf{v}^{opt} that minimizes a given cost functional $F : \mathcal{S} \subset \mathbb{R}^{\tilde{n}} \rightarrow \mathbb{R}$. Besides the cost functional F and the search space \mathcal{S} , the algorithm requires the choice of three parameters. First, the number M of candidate points in \mathcal{S} has to

be chosen. These candidate points constitute the population of solutions. Next, a *differential weight* $\alpha \in (0, 2)$ must be chosen to govern the mutation of three distinct points in \mathcal{S} to obtain a new *donor* point. Finally, a *crossover probability* $C \in (0, 1)$ is prescribed to select entries in a donor point to construct a new candidate point for a better solution in a process called recombination. Once the new candidate point is formed, the value of the functional F at this point is compared to the value at the current point and the new point is used if it improves the functional's value. The algorithm itself is provided in a predecessor paper.¹¹

Let us note that $\tilde{n} = 6$ and $\mathbf{v} = (L, q_L, d_1, d_3, n_1, n_2)$ for the triangle-topped rectangular grating, whereas $\tilde{n} = 4$ and $\mathbf{v} = (L, R, n_1, n_2)$ for the circular grating. For all results presented here, we selected $M = 10\tilde{n}$, $\alpha = 0.8$, and $C = 0.7$.

4. NUMERICAL RESULTS AND DISCUSSION

Our objective was to optimize the geometry of the two splitters shown in Fig. 1 such that

- as much light as possible is transmitted as non-specular Floquet harmonics for $\lambda_0 < \lambda_c$, and
- as much light as possible is transmitted as the specular Floquet harmonic for $\lambda_0 > \lambda_c$.

Since the non-specular Floquet harmonics transport energy in directions different from the specular direction, different energy-harvesting devices can be used for the two spectral regimes.

Accordingly, we set the cost functional

$$F(\mathbf{v}) = \beta \int_{\lambda_{0min}}^{\lambda_{0max}} \left\{ \left[T_{ss}^{(0)}(\lambda_0) - H(\lambda_0 - \lambda_c) \right]^2 + \left[T_{ss}^{n \neq 0}(\lambda_0) - 1 + H(\lambda_0 - \lambda_c) \right]^2 \right\} d\lambda_0 \\ + (1 - \beta) \int_{\lambda_{0min}}^{\lambda_{0max}} \left\{ \left[T_{pp}^{(0)}(\lambda_0) - H(\lambda_0 - \lambda_c) \right]^2 + \left[T_{pp}^{n \neq 0}(\lambda_0) - 1 + H(\lambda_0 - \lambda_c) \right]^2 \right\} d\lambda_0 \quad (17)$$

where the penalty factor $\beta \in (0, 1)$ and

$$H(x) = \begin{cases} 0, & x < 0, \\ 1, & x \geq 0. \end{cases} \quad (18)$$

is the Heaviside step function. The chosen cost functional contains the weighted difference between the transmittance and the Heaviside step function in the L^2 norm. The penalty factor β can be used to tune the functional, but we chose not to explore that issue here and simply set $\beta = 0.5$. We also elected not to penalize the reflectances since by driving the transmittances towards unity we forced the reflectances towards zero.

Although we would like to achieve good separation of specular and non-specular transmissions for a wide range of angles of incidence, the process of averaging F over θ —in addition to averaging over λ_0 —would greatly increase computational time. So we fixed $\theta = 6^\circ$ for optimization, but then explored how the optimal splitters would perform at other angles of incidence. Let us note that $T^{(0)}$, $T^{n \neq 0}$, $R^{(0)}$, and $R^{n \neq 0}$ do not depend on the sign of $\theta \in (-90^\circ, 90^\circ)$, because the unit cells of both candidate splitters are symmetric about the z axis.

For the numerical results presented in this paper, we chose SF11 glass as the material in the half space $z > d$ of transmission. The refractive index n_g as a function of λ_0 is available in the literature.¹³ In addition, we set $n_a = 1$. Both of these choices are consistent with the use of spectrum splitters for solar cells. Fixing $\lambda_{0min} = 450$ nm and $\lambda_{0max} = 950$ nm, we set the wavelength λ_c for the switch between specular and non-specular scattering to be 650 nm. We also assumed $n_{1,2,3}$ to be real and independent of λ_0 , thereby confining the scope of our results to materials with weak dissipation and weak dispersion in the chosen spectral regime. All computational codes were written in Matlab and implemented on a LINUX machine Dell PowerEdge R620 configured with 15K SAS Drives and 320 GB of RAM. Version 2014a of 64bit Matlab was used.

4.1 Optimization of the triangle-topped rectangular splitter

Let us begin with the optimization of the triangle-topped rectangular splitter shown in the left panel of Fig. 1). We set n_3 to be the λ_0 -dependent refractive index of a specific composite material (47% titania and 53% silica) shown in Fig. 2. The following search space \mathcal{S} was fixed:

$$\begin{aligned} L \in [300, 600] \text{ nm}, \quad q_L \in [60, 540] \text{ nm}, \quad d_1 \in [50, 200] \text{ nm}, \\ d_3 \in [50, 200] \text{ nm}, \quad n_1 \in [1, 2], \quad n_2 \in [1, 2]. \end{aligned} \quad (19)$$

We also set $\{L = 500 \text{ nm}, q_L = 250 \text{ nm}, d_1 = 100 \text{ nm}, d_3 = 100 \text{ nm}, n_1 = 1.6, n_2 = 1\}$ as the initial guess for the DEA. As mentioned in Sec. 3, this initial guess was used as one member of the M candidate points in the DEA. The DEA allows the user to set a minimum step size for updating each component of the search space. We use a minimum step size of 10 nm for L , 5 nm for q_L , d_1 and d_3 , and 0.1 for n_1 and n_2 .

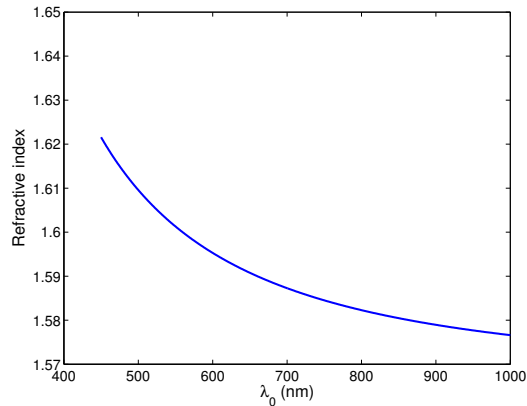


Figure 2. Refractive index n_3 of the composite material containing 47% titania and 53% silica as a function of the free-space wavelength λ_0 .

We obtained the following parameters after 100 iterations of the DEA: $\{L = 600 \text{ nm}, q_L = 360 \text{ nm}, d_1 = 200 \text{ nm}, d_3 = 200 \text{ nm}, n_1 = 1.7, n_2 = 1.0\}$. The progress of the cost functional F towards the optimal design is shown in Fig. 3. The DEA reduced the value of F by approximately 37.7% within just 5 iterations; obviously then, 100 iterations were too many in this case.

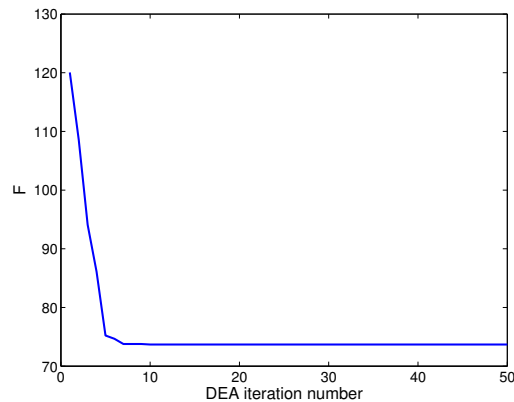


Figure 3. Values of the cost functional F during the first 50 iterations of the DEA for the triangle-topped rectangular splitter. These calculations were done for $\theta = 6^\circ$.

Let us recall that the optimization was done only for $\theta = 6^\circ$. Figure 4 presents the spectrums of $T^{(0)}$, $T^{n \neq 0}$, $R^{(0)}$, and $R^{n \neq 0}$ for $\theta \in \{\pm 6^\circ, \pm 15^\circ\}$ with the initial guess, whereas Fig. 5 presents the same spectrums after 100 iterations of the DEA. Clearly, short-wavelength behavior is much improved and there is a definite switch around $\lambda_c = 650$ nm, as desired. The switch blue-shifts at more oblique incidence, per Fig. 5.

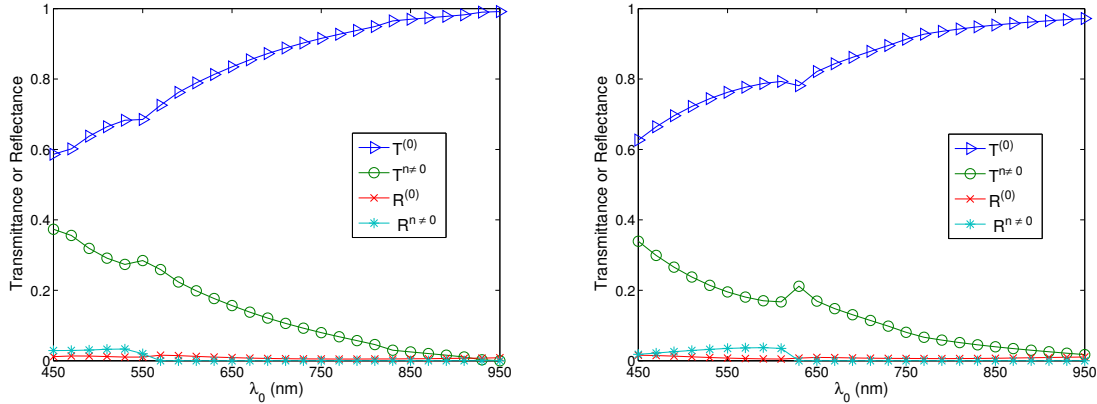


Figure 4. $T^{(0)}$, $T^{n \neq 0}$, $R^{(0)}$, and $R^{n \neq 0}$ as functions of λ_0 for the triangle-topped rectangular splitter described by the initial guess $\{L = 500$ nm, $q_L = 250$ nm, $d_1 = 100$ nm, $d_3 = 100$ nm, $n_1 = 1.6$, $n_2 = 1\}$; (left) $\theta = \pm 6^\circ$ and (right) $\theta = \pm 15^\circ$.

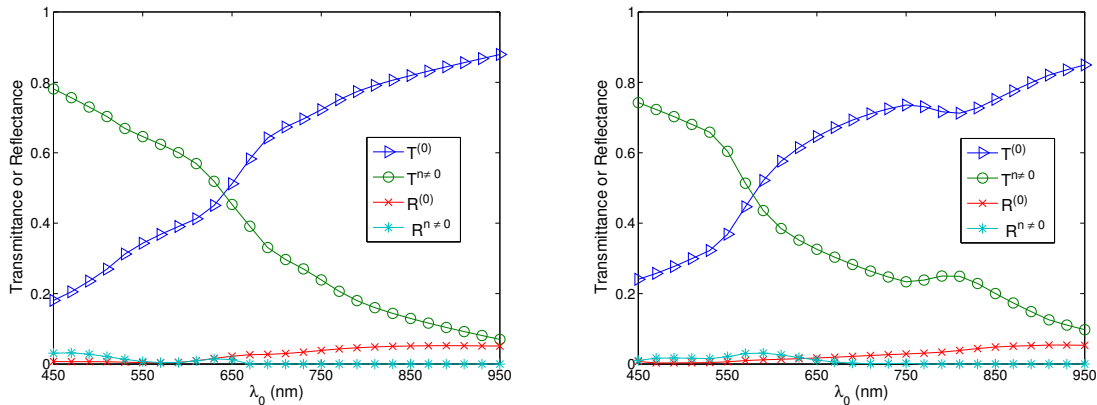


Figure 5. Same as Fig. 4, except for the optimal choice $\{L = 600$ nm, $q_L = 360$ nm, $d_1 = 200$ nm, $d_3 = 200$ nm, $n_1 = 1.7$, $n_2 = 1.0\}$ after 100 iterations of the DEA; (left) $\theta = \pm 6^\circ$ and (right) $\theta = \pm 15^\circ$.

In order to present a complete picture of the behavior of the splitter after 100 iterations of the DEA, in Fig. 6 we present density plots of $T^{(0)}$ and $T^{n \neq 0}$ as functions of θ and λ_0 . Provided that the incidence is not very oblique (say, $|\theta| < 15^\circ$), there is an obvious switch in energy between the specular and non-specular modes of transmission, but this switch occurs at lower wavelengths as the angle of incidence shifts from 0° .

4.2 Optimization for the circular splitter

As the triangle-topped rectangular splitter considered in Sec. 4.1 would be difficult to manufacture, we now turn to the circular splitter shown in the right panel of Fig. 1. Along with $\tilde{n} = 4$ and $M = 40$, the following search space \mathcal{S} was fixed:

$$\begin{aligned} L &\in [300, 600] \text{ nm}, & R/L &\in [0.1, 0.5], \\ n_1 &\in [1.1, 2], & n_2 &\in [1, 2]. \end{aligned} \tag{20}$$

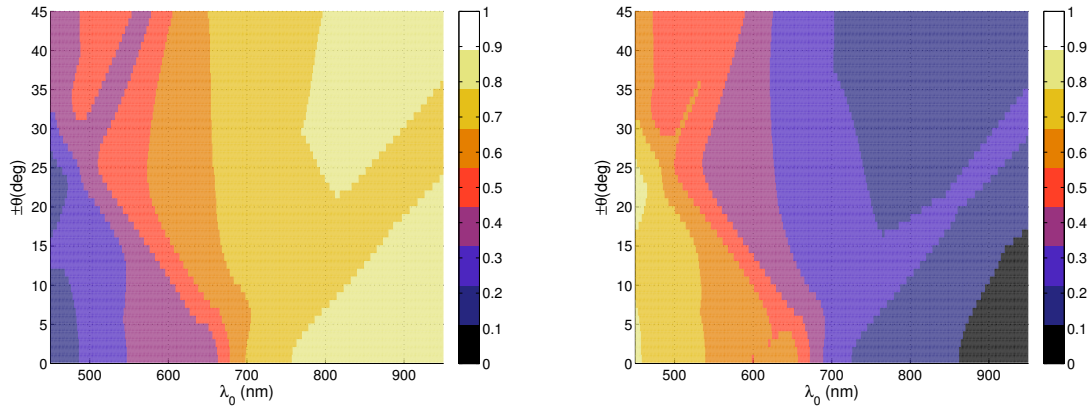


Figure 6. Density plots of (left) $T^{(0)}$ and (right) $T^{n \neq 0}$ against $\theta \in [-45^\circ, 45^\circ]$ and $\lambda_0 \in [450, 950]$ nm for the triangle-topped rectangular splitter after 100 iterations of the DEA.

We also set $\{L = 600 \text{ nm}, R/L = 0.25, n_1 = 1.5, n_2 = 1\}$ as the initial guess for the DEA. We use a minimum step size of 10 nm for L , 0.01 for R/L , and 0.1 for n_1 and n_2 . With these parameters, the reflection and transmission characteristics of the device are shown in Fig. 7. While a tendency towards spectrum splitting is evident, the splitter does not perform well in the short-wavelength regime.

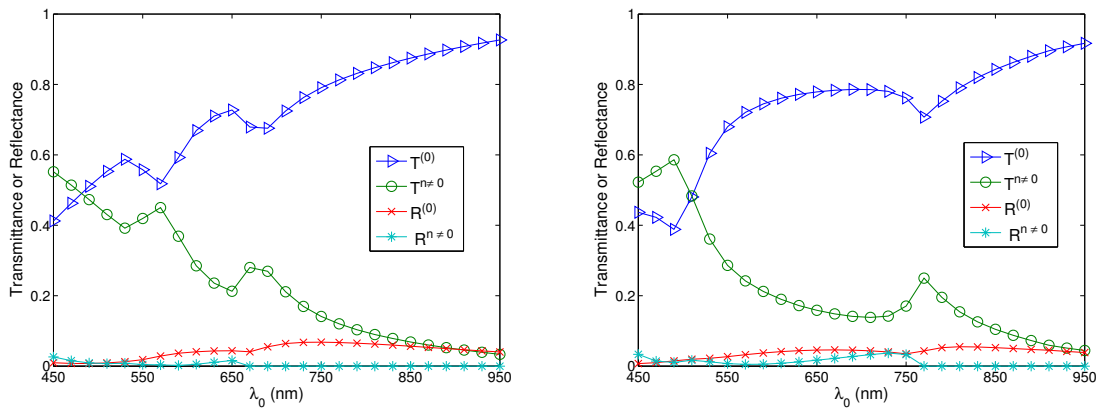


Figure 7. $T^{(0)}$, $T^{n \neq 0}$, $R^{(0)}$, and $R^{n \neq 0}$ as functions of λ_0 for the circular splitter described by the initial guess $\{L = 600 \text{ nm}, R/L = 0.25, n_1 = 1.5, n_2 = 1\}$; (left) $\theta = \pm 6^\circ$ and (right) $\theta = \pm 15^\circ$.

Application of the DEA (with $\theta = 6^\circ$ fixed) provided definite improvement. The progress of the optimization scheme is shown in Fig. 8, the cost functional F decreasing by roughly 18% in 10 iterations and staying flat thereafter. After 100 iterations of the DEA, we obtained the following parameters: $L = 560 \text{ nm}, R/L = 0.3, n_1 = 1.8, n_2 = 1$. With these parameters, the reflection and transmission characteristics of the device are shown in Fig. 9. Despite the relatively small decrease in the cost functional during optimization, the left panel of Fig. 9 ($\theta = \pm 6^\circ$) shows markedly improved short-wavelength behavior with an obvious splitting around λ_c .

In order to investigate the dependence of the splitter's performance on θ , in Fig. 10 we present density plots of $T^{(0)}$ and $T^{n \neq 0}$ as functions of θ and λ_0 . In comparison to the triangle-topped rectangular splitter (Fig. 6), the circular splitter shows poorer splitting for more oblique incidence.

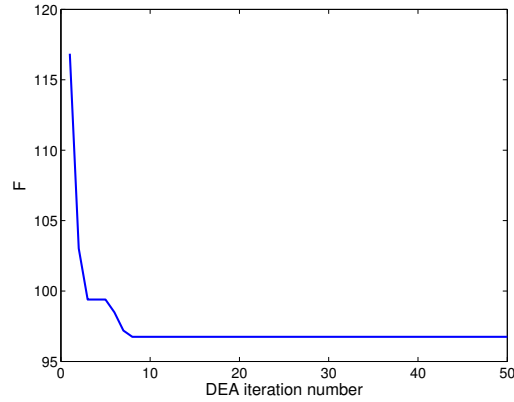


Figure 8. Values of the cost functional F during the first 50 iterations of the DEA for the circular splitter. These calculations were done for $\theta = 6^\circ$.

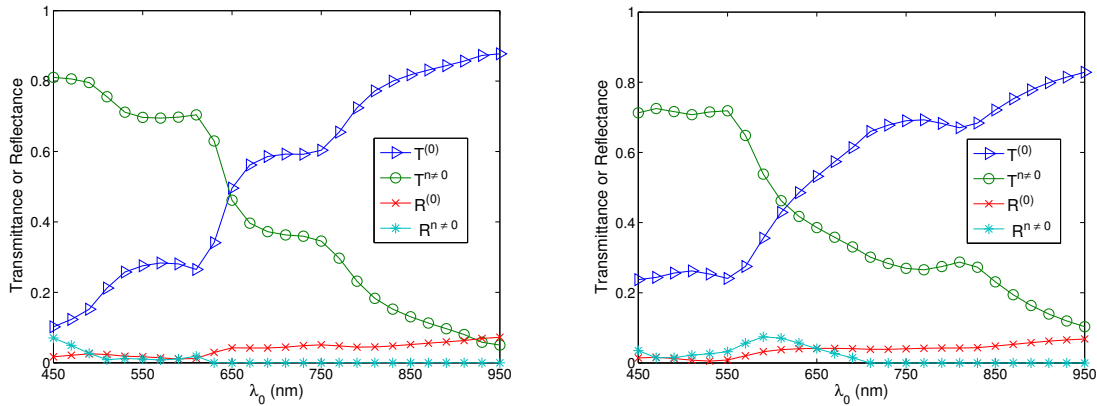


Figure 9. Same as Fig. 7, except for the optimal choice $\{L = 560 \text{ nm}, R/L = 0.3, n_1 = 1.8, n_2 = 1\}$ after 100 iterations of the DEA; (left) $\theta = \pm 6^\circ$ and (right) $\theta = \pm 15^\circ$.

5. CONCLUDING REMARKS

We have demonstrated with two candidate devices that the combination of the RCWA and the DEA is a useful tool for designing surface-relief gratings intended for spectrum splitting. By adjusting a reasonable initial guess, we can optimize the structural and constitutive parameters. Better optimization would require us to allow more changes to the design (e.g., perhaps shapes) but would require more computational time, and might result in structures that are hard to manufacture. We hope that an experimental test of a structure similar to the circular splitter will be forthcoming shortly.

Acknowledgments

Partial support for this work was provided by the US National Science Foundation via Grant No. DMR-1125591. AL acknowledges ongoing support of his research by the Charles Godfrey Binder Endowment at Penn State.

REFERENCES

- [1] Jackson, E.D., "Areas for improvement of the semiconductor solar energy converter," *Proceedings of the Conference on Solar Energy: The Scientific Basis*, University of Arizona, Tucson, AZ, October 31–November 1, 1955. Available at <http://phaidra.univie.ac.at/o:146646>.

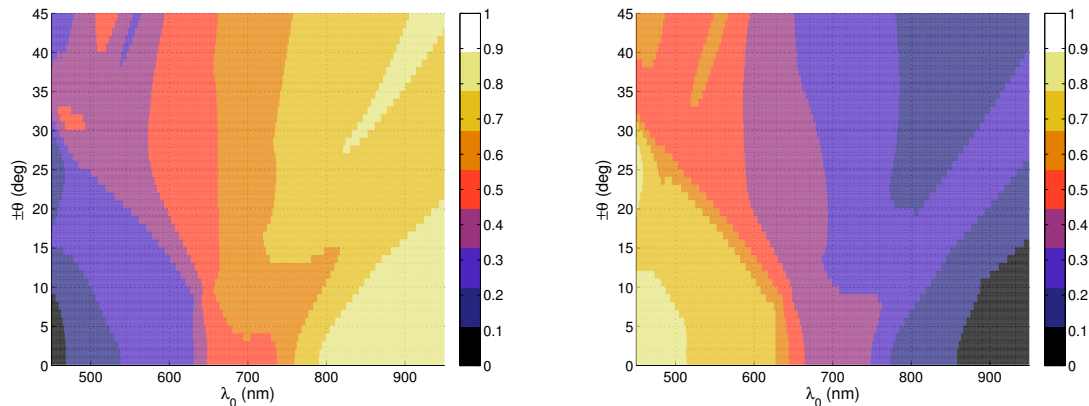


Figure 10. Density plots of (left) $T^{(0)}$ and (right) $T^{n \neq 0}$ against $\theta \in [-45^\circ, 45^\circ]$ and $\lambda_0 \in [450, 950]$ nm for the circular splitter after 50 iterations of the DEA.

- [2] Imenes, A.G. and Mills, D.R., "Spectral beam splitting technology for increased conversion efficiency in solar concentrating systems: a review," *Solar Energy Materials & Solar Cells* **84**, 19–69 (2004).
- [3] Karp, J.H. and Ford, J.E., "Multiband solar concentrator using transmissive dichroic beamsplitting," *Proceedings of SPIE* **7043**, 70430F (2008).
- [4] McCambridge, J.D., Steiner, M.A., Unger, B.L., Emery, K.A., Christensen, E.L., Wanlass, M.W., Gray, A.L., Takacs, L., Buelow, R., McCollum, T.A., Ashmead, J.W., Schmidt, G.R., Haas, A.W., Wilcox, J.R., Van Meter, J., Gray, J.L., Moore, D.T., Barnett, A.M., and Schwartz, R.J., "Compact spectrum splitting photovoltaic module with high efficiency," *Progress in Photovoltaics: Research and Applications* **19**, 352–360 (2011).
- [5] Barber, G.D., Hoertz, P.G., Lee, S.-H.A., Abrams, N.M., Mikulca, J., Mallouk, T.E., Zakeeruddin, S.M., Grätzel, M., Ho-Baillie, A., and Green, M.A., "Utilization of direct and diffuse sunlight in a dye-sensitized solar cell – silicon photovoltaic hybrid," *Journal of Physical Chemistry Letters* **2**, 581–585 (2011).
- [6] Kim, G., Dominguez-Caballero, J.A., Lee, H., Friedman, D.J., and Menon, R., "Increased photovoltaic power output via diffractive spectrum separation," *Physical Review Letters* **110**, 123901 (2013).
- [7] Moharam, M.G., Grann, E.B., and Pommet, D.A., "Formulation for stable and efficient implementation of the rigorous coupled-wave analysis of binary gratings," *Journal of the Optical Society of America A* **12**, 1068–1076 (1995).
- [8] Faryad, M. and Lakhtakia, A., "Grating-coupled excitation of multiple surface plasmon-polariton waves," *Physical Review A* **84**, 033852 (2011).
- [9] Storn, R. and Price, K., "Differential evolution—a simple and efficient heuristic for global optimization over continuous spaces," *Journal of Global Optimization* **11**, 341–359 (1997).
- [10] Price, K.V., Storn, R.M., and Lampinen, J.A., [Differential Evolution: A Practical Approach to Global Optimization], Springer, Berlin (2005).
- [11] Solano, M., Faryad, M., Hall, A.S., Mallouk, T.E., Monk, P.B., and Lakhtakia, A., "Optimization of the absorption efficiency of an amorphous-silicon thin-film tandem solar cell backed by a metallic surface-relief grating," *Applied Optics* **52**, 966–979 (2013).
- [12] Polo Jr., J.A., Mackay, T.G., and Lakhtakia, A., [Electromagnetic Surface Waves: A Modern Perspective], Elsevier, Waltham, MA (2013).
- [13] <http://refractiveindex.info/legacy/?group=GLASSES&material=SF11> (Accessed 20 July 2014).